Journal of Applied Remote Sensing

RemoteSensing.SPIEDigitalLibrary.org

Integrative image segmentation optimization and machine learning approach for high quality land-use and land-cover mapping using multisource remote sensing data

Mohamed Barakat A. Gibril
Mohammed Oludare Idrees
Kouame Yao
Helmi Zulhaidi Mohd Shafri

SPIE.

Mohamed Barakat A. Gibril, Mohammed Oludare Idrees, Kouame Yao, Helmi Zulhaidi Mohd Shafri, "Integrative image segmentation optimization and machine learning approach for high quality land-use and land-cover mapping using multisource remote sensing data," *J. Appl. Remote Sens.* **12**(1), 016036 (2018), doi: 10.1117/1.JRS.12.016036.

Integrative image segmentation optimization and machine learning approach for high quality land-use and land-cover mapping using multisource remote sensing data

Mohamed Barakat A. Gibril,[a,b] Mohammed Oludare Idrees,[a,*] Kouame Yao,[a,c] and Helmi Zulhaidi Mohd Shafri[a]

[a]Universiti Putra Malaysia, Department of Civil Engineering, Faculty of Engineering, Serdang, Selangor Darul Ehsan, Malaysia

[b]University of Prince Mugrin, Department of Civil Engineering, College of Engineering, Madinah, Saudi Arabia

[c]Macquarie University, Department of Earth and Planetary Sciences, Faculty of Science and Engineering, North Ryde, Australia

Abstract. The growing use of optimization for geographic object-based image analysis and the possibility to derive a wide range of information about the image in textual form makes machine learning (data mining) a versatile tool for information extraction from multiple data sources. This paper presents application of data mining for land-cover classification by fusing SPOT-6, RADARSAT-2, and derived dataset. First, the images and other derived indices (normalized difference vegetation index, normalized difference water index, and soil adjusted vegetation index) were combined and subjected to segmentation process with optimal segmentation parameters obtained using combination of spatial and Taguchi statistical optimization. The image objects, which carry all the attributes of the input datasets, were extracted and related to the target land-cover classes through data mining algorithms (decision tree) for classification. To evaluate the performance, the result was compared with two nonparametric classifiers: support vector machine (SVM) and random forest (RF). Furthermore, the decision tree classification result was evaluated against six unoptimized trials segmented using arbitrary parameter combinations. The result shows that the optimized process produces better land-use land-cover classification with overall classification accuracy of 91.79%, 87.25%, and 88.69% for SVM and RF, respectively, while the results of the six unoptimized classifications yield overall accuracy between 84.44% and 88.08%. Higher accuracy of the optimized data mining classification approach compared to the unoptimized results indicates that the optimization process has significant impact on the classification quality. [DOI: 10.1117/1.JRS.12.016036]

Keywords: segmentation; remote sensing; fusion; land use and land cover; Taguchi optimization; data mining.

Paper 170883 received Oct. 10, 2017; accepted for publication Feb. 16, 2018; published online Mar. 9, 2018; corrected Mar. 13, 2018.

1 Introduction

Fusion of optical and SAR images has been extensively used to improve the quality of feature extraction in many applications. The advantages of combining multisource spatial data to enhance land use and land cover (LULC) classification have been widely reported.[1–6] However, the quality of the extracted information also relies on the classification algorithm.[7] Today, geographic object-based image analysis (GEOBIA) has become the normative feature extraction approach for the remote sensing community, a paradigm shift from the conventional

*Address all correspondence to: Mohammed Oludare Idrees, E-mail: dare.idrees@gmail.com

1931-3195/2018/$25.00 © 2018 SPIE

pixel-based image classification method.[8–10] GEOBIA permits multiscale and hierarchical image object representation with additional benefits of employing knowledge-driven mechanisms using the image semantics, such as spectral, spatial texture, and contextual information.

Object-based mapping techniques are even more desirable to generate informative and accurate maps when data from different sensors are combined. Data fusion is a popular technique in remote sensing; however, studies to combine data for object-oriented approach have always relied on the standard fusion techniques, such as wavelet transform, bravery, HIS (intensity hue and saturation), pan-sharpening, Ehlers etc.[2,4,11–14] Although these fusion techniques enhance spatial resolution of the resulting image, it is well documented that they suffer from spectral distortion.[4,15] Also, there is limitation in the number of data that can be combined. Nevertheless, improvement in feature extraction and mapping through fusion and object-based techniques has been reported for various applications, including urban land cover,[13,16] landslide inventory and mapping,[11,17] vegetation mapping,[5,18,19] and flood extent extraction.[14] More recently, the idea of integrating spectral and nonspectral information to enrich feature attributes extraction for better classification and quality map production has been advanced.[8] In line with this development and the growing application of machine learning algorithms,[4,13] fusion by layer stacking is gaining prominence in remote sensing image analysis.[3,20,21]

Image segmentation is the foundation of GEOBIA. The segmentation process divides image into smaller nonoverlapping regions using the color, texture, and shape properties of the image, usually governed by three parameters available to users, namely scale, shape, and compactness.[22,23] The process of identifying optimum combination of these parameters is very challenging.[24] Thus, using an optimization technique can be very effective to reduce time and effort involved in a trial-and-error strategy and also to improve feature detection accuracy. Various strategies have been used to evaluate the segmentation quality, including visual analysis, system-level evaluation, empirical discrepancy methods, and empirical goodness methods.[16,25]

The first method employs visual analysis by comparing multiple segmentation outputs to select best parameter combination. But the approach is subjective, time-consuming, and does not include any quantitative measure to evaluate the quality. The second method is at system-level, which considers segmentation as major part of classification that directly affects the final result. It evaluates quality using classification accuracy as indicator.[26–28] The third one is the empirical discrepancy method, which references the polygons (e.g., manually digitized features) to examine optimal combination of parameters by measuring the discrepancies between segmentations output and the digitized image objects. If the discrepancy between the segmentation and reference objects is minor, it indicates high segmentation quality.[12,16,26,29–34] The drawbacks of this technique include the need for extensive manual effort to prepare the reference objects, which can be subjective, labor, and time-consuming.

The last quality evaluation method is empirical goodness methods.[29] The empirical goodness methods involve the adoption of statistical quality criteria to score and rank multiple image segmentation and find the optimal combination of segmentation parameters.[25] An empirical goodness objective function proposed by Espindola et al.[35] uses quantitative statistical criterion that combines the weighted variance and spatial autocorrelation (Moran's index) of the image pixels to determine segmentation quality. A plethora of empirical goodness methods was proposed and tested.[25,27,33,36–39] The issue with these empirical methods is that they only optimize the scale parameter and do not emphasize on finding the optimal combination of the three parameters.[40,41]

The robust Taguchi statistical technique, a fractional factorial design, established by Genichi Taguchi has been widely adopted in the engineering analysis to optimize the design variables and the performance characteristics of the combination of design parameters.[42] It provides a straightforward and efficient tool to find the optimum ranges of designs for a high-quality system and significantly minimize the overall testing time and experimental cost.[43] It uses an orthogonal array from the design of the experiment that provides a straightforward and systematic method to optimize the design and assesses the performance by measuring signal to noise ratio (SNR) of each experiment. The merger of Espindola's objective function and Taguchi optimization technique has been applied recently and is gaining relevance in remote sensing applications, such as landslide inventory mapping,[40,17] flood mapping,[14] asbestos cement roofs detection,[20] and automatic birds' nests detection and counting.[41] In this study, LULC classification was improved

using GEOBIA. First, segmentation is optimized using Taguchi statistical technique and, subsequently, classification carried out using the machine learning C4.5 decision tree algorithm. Then, the proposed method is compared with support vector machine (SVM; optimized with Taguchi statistical technique), random forest (RF), and a set of unoptimized trials segmented using arbitrary parameter combinations to investigate efficiency of the optimization process.

2 Study Area, Data, and Method

The study was conducted in Perak, a state in Peninsula Malaysia. Geographically, the site is located between longitudes 100°51′22″E and 101°14′17″E, and latitudes 4°13′21″ N and 3°51′60″N (Fig. 1), covering ∼1741.5 km^2. The land use comprises residential settlements, water bodies, and agricultural land, including oil palm, rice paddy, and vegetable crops.

SPOT-6 and RADARSAT-2 imageries used in this study were provided by Agensi Remote Sensing Malaysia (ARSM). The SPOT-6 image, which was acquired in February 2014, has 6-m spatial resolution and four multispectral bands within 0.455- to 0.890-μm wavelength. Similarly, the RADARSAT-2 image was acquired on March 15, 2015, using fine beam mode SGF with HH

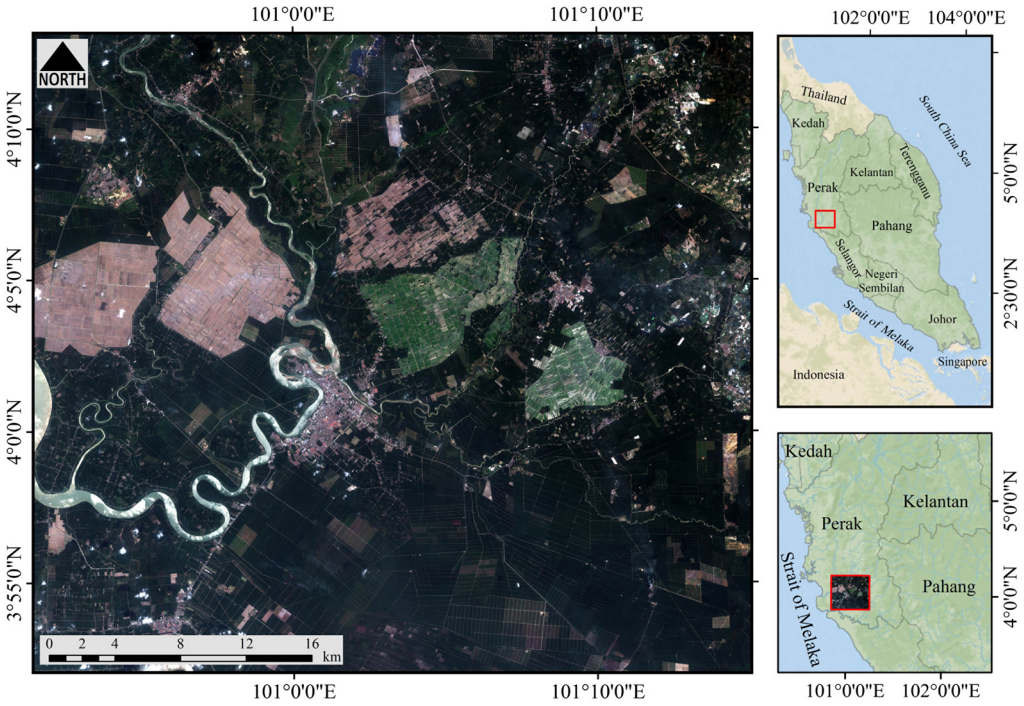

Fig. 1 Study area with Malaysian states and the location of the study area (right map) and SPOT-6 imagery in RGB color combinations (left image).

Table 1 Data used and their properties.

Properties	SPOT-6	RADARSAT-2
Acquisition date	February 2, 2014	March 15, 2015
Spatial resolution (m)	6 m	12.5 m
Wavelength	0.455 μm to 0.525 μm blue 0.530 μm to 0.590 μm green 0.625 μm to 0.695 μm red 0.760 μm to 0.890 μm NIR	C-band
Polarization	—	HH

single polarization at 20-deg to 50-deg incidence angle. The SAR image was terrain geocoded and resampled to 12.5 m on delivery. Table 1 presents the characteristics of the dataset.

2.1 *Data Processing*

For the preprocessing task, SPOT-6 image was corrected for radiometric and atmospheric effects. Also, speckle in the SAR data was removed using 5×5 kernel local sigma. Subsequently, the image was enhanced texturally with 3×3 kernel textural occurrence and resampled to 6-m spatial resolution to match SPOT-6 image. The two datasets were coregistered to bring them into correct alignment using image-to-image registration. Thereafter, the images were reprojected to Universal Transverse Mercator projection. Then, the two datasets were fused by layer stacking. Unlike other fusion methods that transform the image spectral, layer stacking combines dataset from different sensors without altering the spatial and spectral characteristics of the original data.[1] This ability to retain the image fidelity is an advantage for object-based image analysis because the algorithm exploits all image properties to detect physical object in the image.

2.2 *Optimization and Segmentation*

Then, the segmentation process was optimized using integrated Taguchi-objective function optimization strategy.[41] Based on the optimal parameter combinations, the image was segmented and the result classified using different algorithms, including data mining (DM) using a developed rule-set. Finally, the effect of the optimization was evaluated. Figure 2 presents the data processing and analysis workflow.

Image segmentation is the first and most fundamental step in GEOBIA.[27] The widely used region growing multiresolution segmentation (MRS) was employed. MRS starts with a single-pixel image object as seed, and then other neighboring image pixels are combined in several successive steps to produce larger ones till the predefined criteria are met.[44] However, the quality of this process depends on the proper selection of segmentation parameters: scale and homogeneity (shape and compactness) values. The scale value controls the size segment: high-scale value produces large image segment and small-scale value generates small segments.[10,45] The other parameters, homogeneity, combine color and shape properties. In this research, the robust Taguchi-objective function optimization technique was used to derive appropriate parameter combination for the scale, shape, and compactness.[11,14,40,41,17,20] The technique integrates the statistical Taguchi and spatial objective function optimizations methods iteratively in a single processing workflow to produce an accurate result.

In GEOBIA, segmentation of image spectral relative to their spatial arrangement (autocorrelation) is fundamental to feature identification and grouping. The segmentation technique divides image into homogeneous contiguous regions that enclose identical pixels as objects within each segment based on the assumption that an image pixel most likely belongs to the same object as its neighboring pixels.[46] Accurate partitioning of image into distinct image objects is dependent on appropriate selection of segmentation parameters: scale, shape, and compactness. Over the time, the objective function,[47] which attempts to select appropriate parameters that can produce the best quality segmentation based on intrasegment homogeneity and intersegment reparability, has been widely used. However, this optimization technique relies on arbitrary selection of a range of parameters for experimentation. Not only that, it emphasizes on varying the scale factor while keeping the shape and compactness factors constant, even though the quality of the resulting segments depends on the correct combination of the three parameters. And this is perceived as bias for the objective function. Hence, the idea of incorporating Taguchi method into the optimization process by, first, optimizing the design of experiment using the Taguchi orthogonal array and, second, modeling a unique optimal parameter combination with the Taguchi SNR is presented. Comprehensive details of this approach can be found in literature.[41,48,49]

For experimental design, five levels were defined for the three segmentation parameters (Table 2). The orthogonal array minimizes the number of experiments to only 25 number of experiment coded L25 (3^5) compared to 243 experiments using the standard factorial. The plateau objective function (POF)[35] was measured for each experiment to evaluate the quality of the

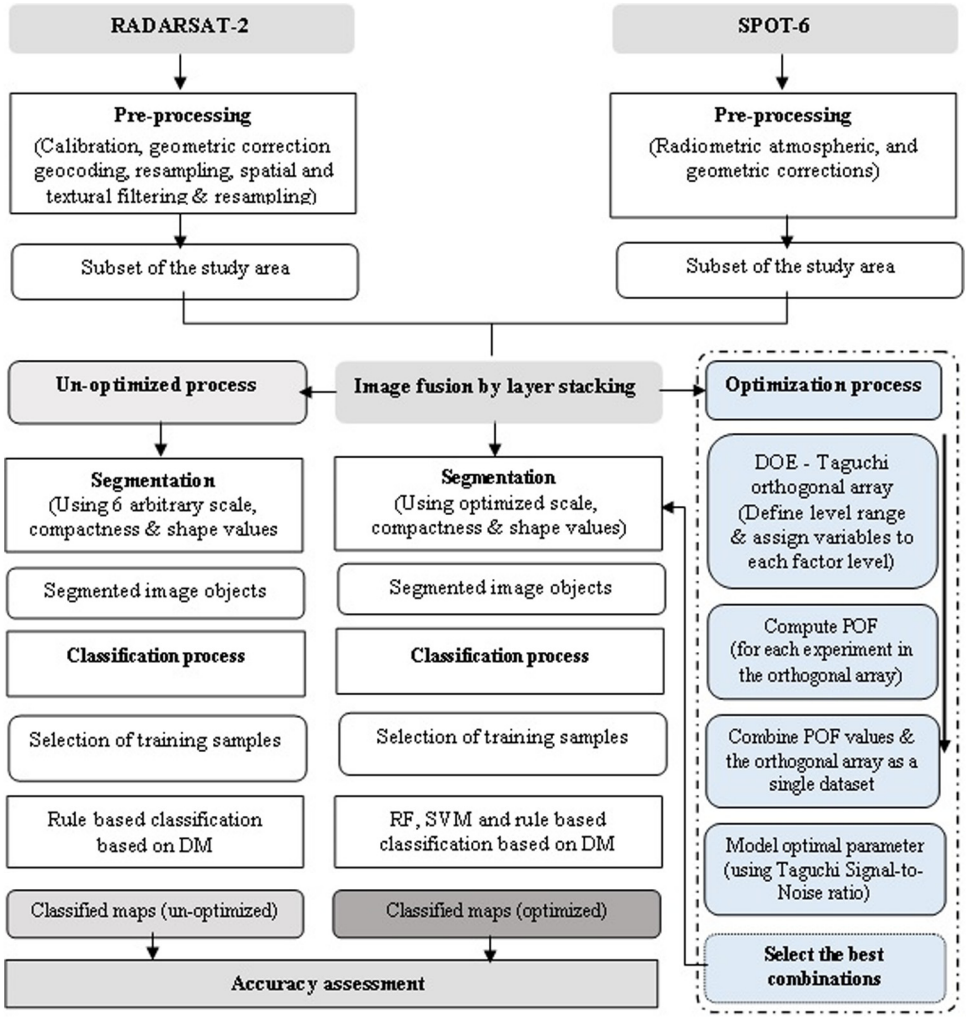

Fig. 2 Methodological workflow.

Table 2 Segmentation parameter level and variable definition.

Level	Scale	Shape	Compactness
1	30	0.5	0.1
2	40	0.6	0.3
3	50	0.7	0.5
4	60	0.8	0.7
5	70	0.9	0.9

segmentation for each experiment. POF is a combination of the weighted variance and spatial autocorrelation (Moran's index) to evaluate both of the intersegment homogeneity and heterogeneity of image objects. To assess experimental results, SNR is calculated as a measure for the determination of the quality. The SNR values yield the optimum segmentation parameters, which were used for image segmentation, followed by classification to extract land-cover classes. Different land-cover features were correctly classified by exploiting the spectral, textural, and spatial relationship of the image objects (segments).

2.3 *Classification and Accuracy Assessment*

The outcome of segmentation is an unclassified image object with database of the layer values, such as spectral indices, backscattering values, and textural parameters (Table 3) that allows manipulating the feature characteristics for DM. The optimized image objects generated was classified into nine land-cover classes (palm oil, initial paddy stage, intermediate paddy stage, matured paddy stage, bare soil, flooded soil, built up areas, water bodies, and grass

Table 3 Description of the feature space included in SVM, RF, and rule-based classification to classify image objects derived from multisource data and optimized by Taguchi technique.

Feature types	Feature names and descriptions
Spectral	Mean reflectance band of blue, green, red, NIR, and backscattering.
	The standard deviation of reflectance band of blue, green, red, NIR, and backscattering.
	Normalized difference vegetation index $[\frac{(R_{NIR}-R_{Red})}{(R_{NIR}+R_{Red})}]$.
	Normalized difference water index $[\frac{(R_{Green}-R_{NIR})}{(R_{Green}+R_{NIR})}]$.
	Soil adjusted vegetation index $[\frac{(R_{NIR}-R_{Red})}{(R_{NIR}+R_{Red}+l)} * (1+L)]$.
	Ratio *G* index[56] $= \frac{R_{Green}}{(R_{Blue}+R_{Green}+R_{Red}+R_{NIR})}$.
	Brightness values.
Textural	grey level co-occurrence matrix (GLCM) mean, GLCM contrast, GLCM entropy, GLCM dissimilarity, GLCM homogeneity, GLCM correlation, GLCM std., GLCM Ang. second moment, grey level difference vector (GLDV) mean, GLDV contrast, GLDV entropy, and GLDV Ang. second moment.
Spatial and geometric	Density, compactness, asymmetry, shape index, rectangular fit, and elliptic fit.

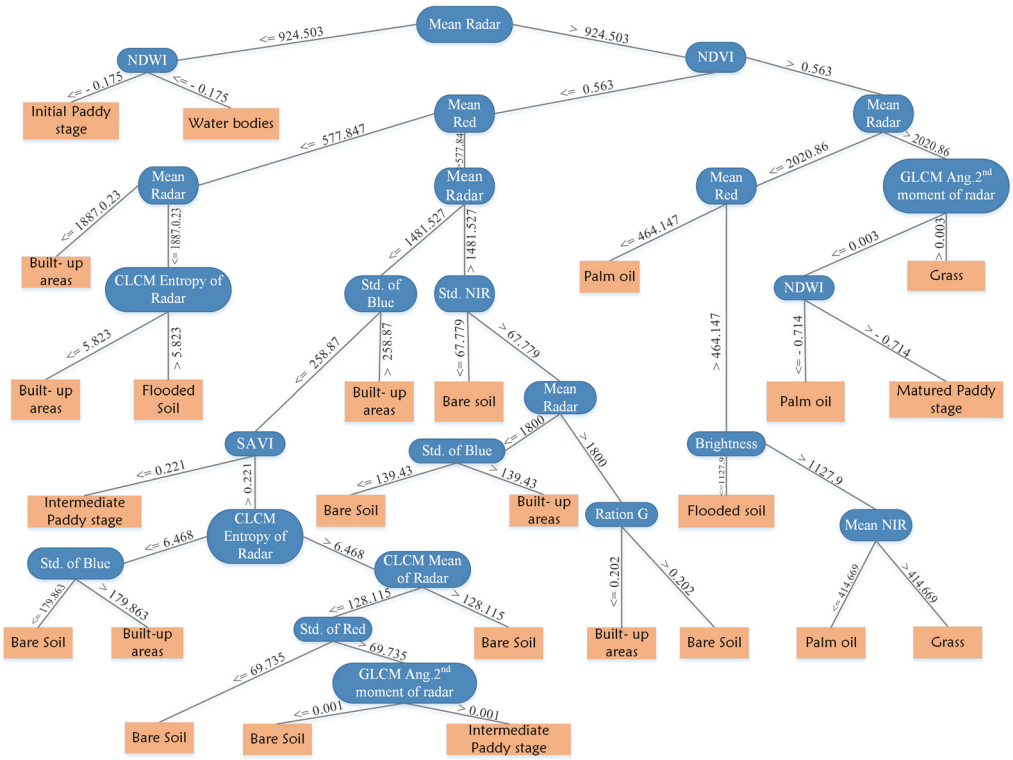

Fig. 3 Decision tree generated in Weka for developing russets used for the classification.

or other vegetation) using SVM, RF, and rule-based DM approach. Theoretical bases of SVM, RF, and DM can be found in literature.[13,19,18,50–55]

SVM and RF classifiers were applied by selecting training samples representative of the respective feature class. But for the rule-based classification, decision tree (Fig. 3) was constructed by implementing the C4.5 algorithm in Weka,[55] an open source software using the image object attributes and indices (Table 3). The defined relationships between the image attributes and land-cover classes were utilized in building rule-sets for classifying the image objects. Performance of the optimization process was evaluated by comparing its result with six different studies in which their segmentation parameters were arbitrarily combined and classified using the rule-based classification method. Evaluation of the classifiers was based on the classification accuracy using the traditional confusion matrix and its measures (overall accuracy, kappa coefficient, etc.).[57] Selection of training image objects for classification and accuracy assessment was

Table 4 L25 orthogonal array for MRS and SVM parameters and experiments responses.

	L25 combination of MRS parameters				L25 combination of SVM parameters		
Experiment	Level	Shape	Compactness	POF	C	γ	Kappa
1	30	0.5	0.1	1	10	0.1	0.78
2	30	0.6	0.3	1.0001	10	0.3	0.80
3	30	0.7	0.5	1.1358	10	0.5	0.78
4	30	0.8	0.7	1.2186	10	0.7	0.79
5	30	0.9	0.9	1.3166	10	0.9	0.78
6	40	0.5	0.3	1.1841	30	0.1	0.80
7	40	0.6	0.5	1.2618	30	0.3	0.82
8	40	0.7	0.7	1.3595	30	0.5	0.85
9	40	0.8	0.9	1.3901	30	0.7	0.85
10	40	0.9	0.1	1.2895	30	0.9	0.83
11	50	0.5	0.5	1.3786	50	0.1	0.80
12	50	0.6	0.7	1.5315	50	0.3	0.84
13	50	0.7	0.9	1.4264	50	0.5	0.85
14	50	0.8	0.1	1.4821	50	0.7	0.85
15	50	0.9	0.3	1.0454	50	0.9	0.83
16	60	0.5	0.7	1.5421	70	0.1	0.82
17	60	0.6	0.9	1.5149	70	0.3	0.87
18	60	0.7	0.1	1.5327	70	0.5	0.85
19	60	0.8	0.3	1.2681	70	0.7	0.85
20	60	0.9	0.5	1.0814	70	0.9	0.83
21	70	0.5	0.9	1.4635	90	0.1	0.82
22	70	0.6	0.1	1.525	90	0.3	0.87
23	70	0.7	0.3	1.3883	90	0.5	0.86
24	70	0.8	0.5	1.1012	90	0.7	0.85
25	70	0.9	0.7	0.8548	90	0.9	0.83

done randomly. The GPS points collected during the site visit does not cover the entire range of classes defined in this study due to the coverage and accessibility. Therefore, the process of selecting training samples was guided by the GPS points, the land-use map provided by the Town and Country Planning Department and GoogleEarth image. In addition, quantitative assessment was carried out to know whether there is a significant change in the classification accuracy result before and after optimization using McNemar's tests.[58]

3 Results and Discussion

3.1 *Optimization Output*

The first two stages of optimization derived from the 25 experiments produced a preliminary view of some level of optimization for the MRS and SVM parameters, where the POF and kappa values are indicators (Table 4). However, at this level, the operation still pose some challenges of the correct choice of optimal combination because there are a number of closely related POF and kappa from different combinations that seems optimal.

But further iteration using SNR "larger is better" option provided refined optimal values (Fig. 4 and Table 5) that eliminates the ambiguity discussed above. Ultimately, the results yield optimum parameter combination 60:0.7:0.9 for the scale, shape, and compactness factors, respectively, for the MRS and 90 and 0.3 for C and γ, respectively, for SVM.

3.2 *Classification Results and Accuracy*

Classification results for the optimized (SVM, RF, and DT) and unoptimized (DT) segmentations processes are presented in Figs. 5 and 6. Each classified image contain nine classes: palm

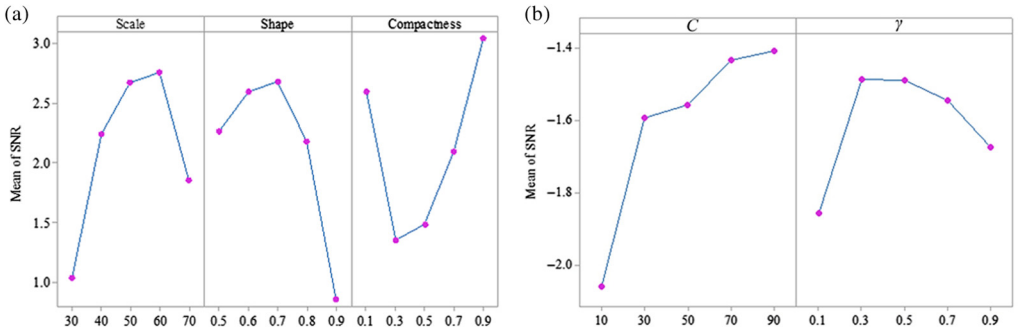

Fig. 4 Main effect plot of the SNR "larger is better" for (a) MRS and (b) SVM parameters.

Table 5 Statistical SNR evaluations for MRS and SVM parameters.

	MRS			SVM	
Level	Scale	Shape	Compactness	C	γ
1	1.0427	2.2652	2.6001	−2.059	−1.856
2	2.2448	2.5992	1.3534	−1.593	**−1.486**
3	2.6758	**2.6835**	1.4862	−1.557	−1.489
4	**2.7643**	2.1792	2.0974	−1.434	−1.544
5	1.8595	0.86	**3.0501**	**−1.408**	1.675
Delta	1.7216	1.8235	1.6968	0.651	0.37
Rank	2	1	3	1	2

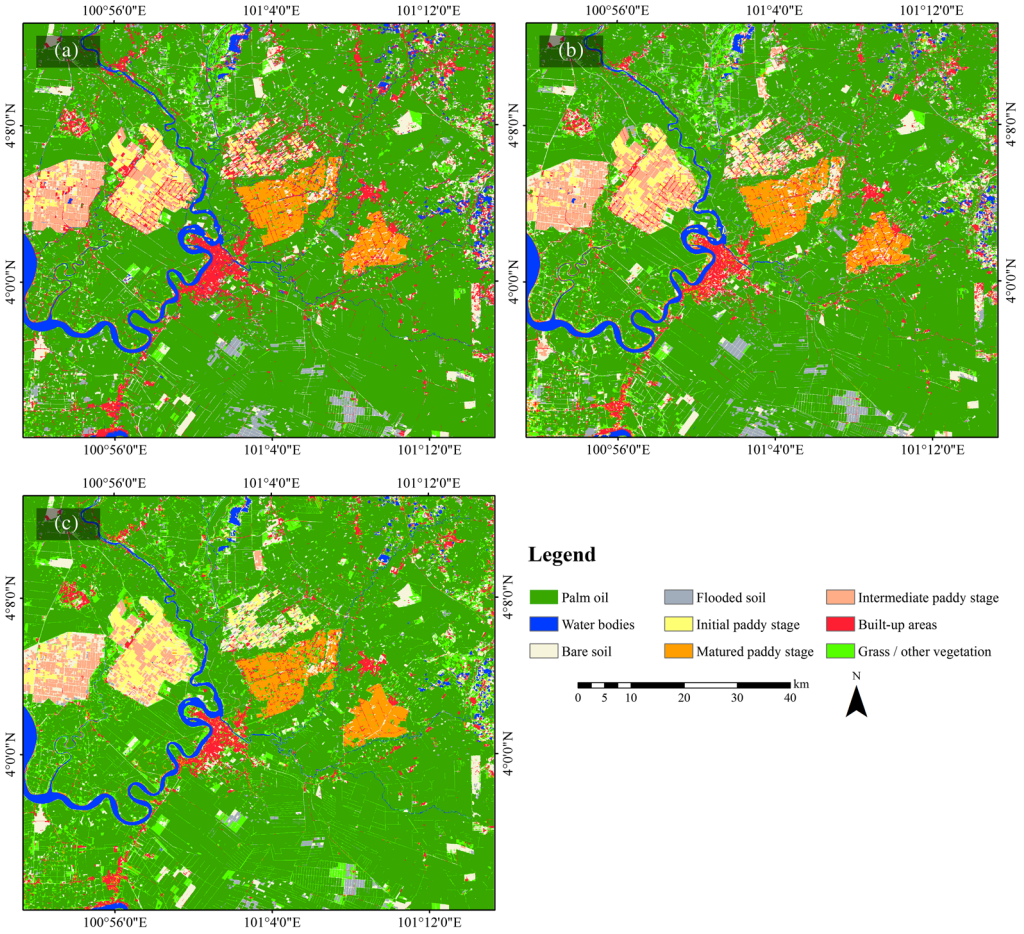

Fig. 5 LULC map using the optimized segments: (a) SVM, (b) RF, and (c) machine learning-based DT.

oil, initial paddy stage, intermediate paddy stage, matured paddy stage, bare soil, flooded soil, built up areas, water bodies, and grass or other vegetation types.

Qualitatively, the use of multiattributes of the surface characteristics using the images and their derivatives enhanced the quality of the resulting map. Particularly, in tropical agricultural areas, integration of optical and radar sensor data has provided additional information to separate intraspecies vegetation and various land-cover classes.[3,5,59] The classification maps obtained from the optimized SVM, RF, and DM classifiers do not show much difference except for the flooded soil class in the southern part of the image, which is well classified in SVM and RF and partly misclassified as grass/other vegetation in DM. Aside this class, DM shows superiority in identifying subtle features as can be seen in the lot demarcation boundaries and road network, most of which are not detected in SVM and RF. The HH polarization is highly sensitive to moisture content and vegetation;[5] these accounts for the well-classified vegetation types. Also, the rivers and their tributaries are well mapped in SVM and DM; but further away from the main river, the tributaries were not detected in RF. Visual analysis reveals that SVM and RF exhibit misclassification among built-up area, bare soil, and matured paddy classes and also between flooded soil and grass land, particularly within the paddy fields, all of which are distinctively separated into their respective classes with DM classifier.

Quantitative evaluation of the classification yielded overall classification accuracy of 87.25%, 88.69%, and 91.79% for SVM, RF, and DM, respectively (Table 6). The accuracy obtained is similar to the result obtained with closely related works. For example, Zhang and Xie[19] obtained classification accuracy of 85% and 89% with SVM and RF, respectively, after fusion. Similarly, Ribeiro and Fonseca[13] obtained an overall accuracy of 85.66% from pan-sharpened WorldView-2 using object-oriented techniques and DT classifier. On a scale

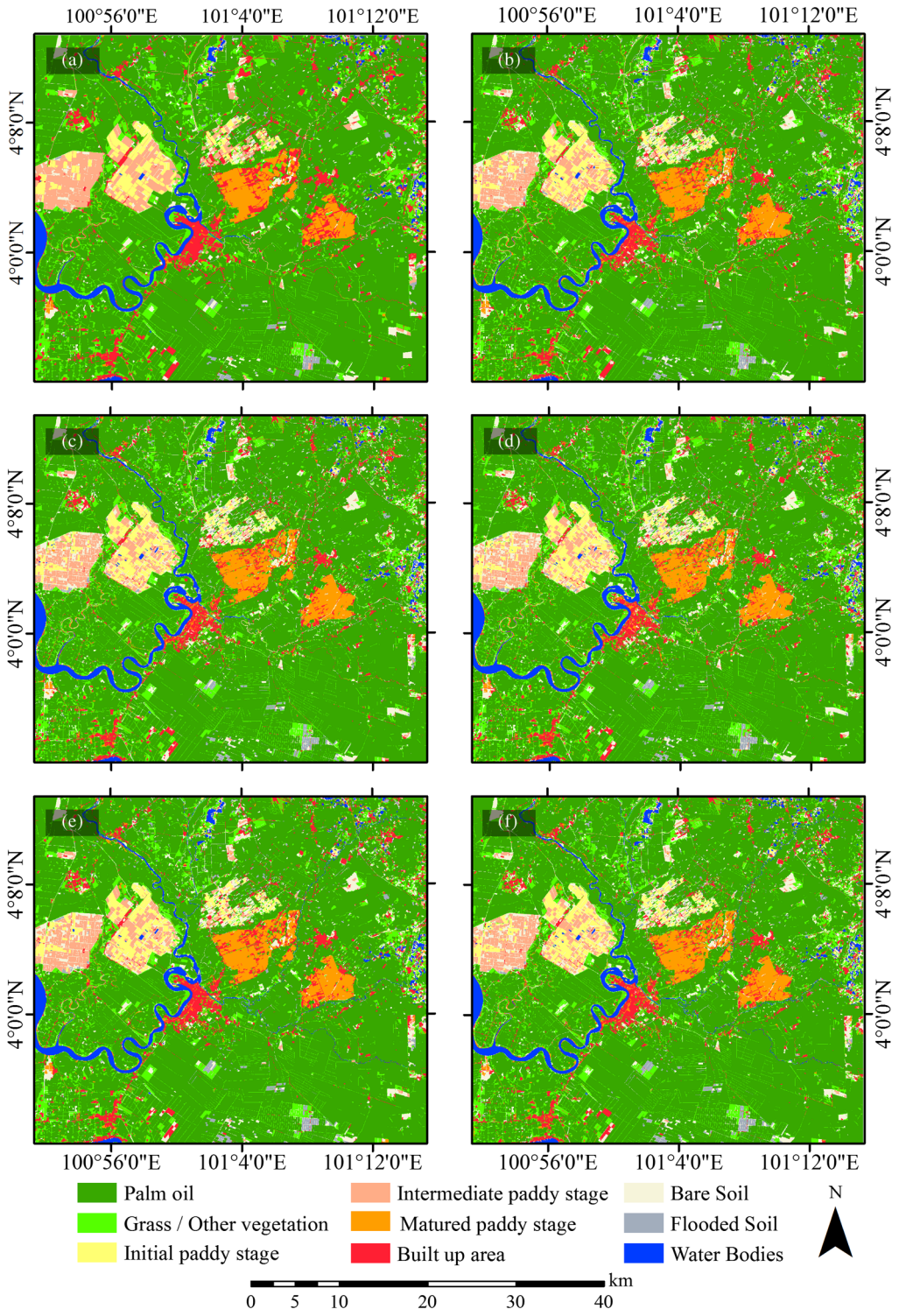

Fig. 6 Classification results of the unoptimized process using arbitrary segmentation parameter combinations (a) 100, 0.9, 0.3; (b) 90, 0.7, 0.3; (c) 80, 0.7, 0.5; (d) 70, 0.7, 0.7; (e) 60, 0.9, 0.5; and (f) 50, 0.9, 0.1.

of performance, the three maps produced acceptable results; however, DM using decision-based approach produces superior quality.

Classification maps produced from the unoptimized segmentation show somewhat a similar result with obvious misclassification of the matured paddy class as built-up area. This phenomenon is much pronounced for the larger scale categories (i.e., 100, 90, and 80); but as the scale

reduces, so also the degree of misclassification reduced. In all the outputs, the main water bodies are well represented, but most of the tributaries are misclassifies as built-up area, intermediate paddy, or bare-soil [Figs. 6(a)–6(e)], whereas at scale 50 [Fig. 6(f)], the tributaries are correctly classified as water. This indicates that using large scale could result in grouping two or more features in a segment (under segmentation), conversely, if the scale is too small it will lead to

Table 6 Error matrix for SVM, RF, and DT classifiers with UA and PA.

	SVM		RF		Rule-based based on DM	
Class	PA (%)	UA (%)	PA (%)	UA (%)	PA (%)	UA (%)
Palm oil	92.21	96.2	98.01	96.01	**96.99**	**92.41**
Initial paddy	96.58	95.47	98.37	85.07	**98.41**	**79.59**
Intermediate paddy	67.54	100	86.72	88.42	**90.58**	**96.98**
Matured paddy	89.59	99.71	84.08	96.06	**92.36**	**80.59**
Grass	86.73	100	86.47	96.16	**86.32**	**99.91**
Bare soil	94.05	76.88	77.42	81.64	**78.09**	**92.21**
Flooded soil	91.57	58.99	99.81	68.29	**90.87**	**89.00**
Built up areas	96.1	72.63	90.12	91.52	**98.34**	**88.67**
Water bodies	90.48	83.54	86.03	82.99	**96.92**	**100.00**
Overall accuracy	87.25		88.69		**91.79**	
Kappa	0.87		0.87		**0.90**	

Note: Values in bold face indicate the best result.

Table 7 Classification accuracy of the unoptimized parameter combination.

	100, 0.9, 0.3		90, 0.7, 0.3		80, 0.7, 0.5		70, 0.7, 0.7		60, 0.9, 0.5		50, 0.9, 0.1	
	PA (%)	UA (%)	PA (%)	UA (%)	PA (%)	UA (%)	PA (%)	UA (%)	PA (%)	UA (%)	PA (%)	UA (%)
Palm oil	95.07	93.23	93.16	88.97	95.07	88.83	95.07	88.8	92.62	93.34	95.01	91.97
Initial paddy	81.44	74.42	84.4	98.3	77.49	98.23	79.88	73.58	86.95	98.27	79.38	97.59
Intermediate paddy	89.51	88.55	86.88	86.94	81.27	89.62	81.35	93.48	86.06	90.1	85.1	91.32
Matured paddy	80.38	78.26	88.7	79.39	90.51	79.03	86.98	79.04	92.57	80.34	82.83	77.39
Grass	88.75	85.89	80.59	83.34	79.58	86.72	79.64	91.49	88.67	86.94	86	92.96
Bare soil	73.76	94.44	66.92	81.1	67.86	81.88	69.69	84.62	76.07	92.12	74.95	83.89
Flooded soil	70.51	99.8	89.51	88.85	78.37	66.45	86.42	67.1	77.2	67.36	98.31	83.07
Built-up areas	95.64	73.31	96.51	81.54	97.3	80.87	89.59	72.87	95.84	83.38	93.54	78.1
Water bodies	89.27	100	88.45	94.71	90.46	86.71	89.27	91.69	90.91	91.36	90.57	87.62
Overall accuracy	86.93%		86.16%		85.04%		84.44%		88.08%		87.06%	
Kappa coefficient	0.85		0.84		0.828		0.822		0.863		0.8513	

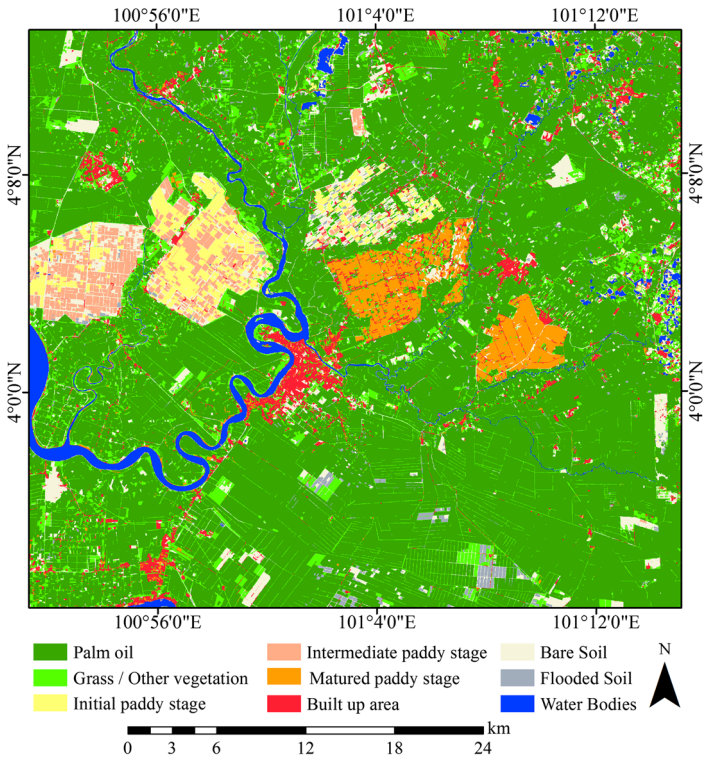

Fig. 7 Final LULC map generated from the optimization process and DT classifier.

over segmentation, which could equally complicates the classification process.[32,33,60] The trend in the visual analysis is reflected in the quantitative evaluation results (Table 7).

In Table 7, it can also be observed that the classification accuracy of the unoptimized segmentation performs well, with the overall accuracy range between 84.44% and 88.08% for both SVM and RF, respectively. However, the optimized DT result out performed them all. On the basis of this, the optimized DT classification output was selected as the best for the LULC map (Fig. 7). Statistically, the McNemar's computed (two-sided) $p < 0.0001$ is less than the conventional 0.05 at 95% CI, we cannot accept the null hypothesis. Therefore, the conclusion is that there is a significant difference between the optimized and unoptimized classification processes. In general, optimization significantly improved the quality of the classification; however, careful selection of segmentation parameter combination can also produce acceptable result, as demonstrated in Table 7. Inability to obtain sufficient independent ground data for the evaluation process may affect the result; nonetheless, the use of the basic map provided and GoogleEarth image is adequate for this task. Decision tree based on DM provides better qualitative LULC classification map with the optimized segmentation.

4 Conclusion

Advances in information and data science are fast unifying different disciplines in exploratory knowledge-based applications. In the field of remote sensing, there is growing use of machine learning algorithms for complex decisions. The process translates human cognition to machine intelligence in a more sophisticated way. This study demonstrates a key application in LULC mapping. GEOBIA enables obtaining all rich information from the images to be mined. Combination of segment optimization and DM will increase the accuracy and reliability of feature extraction even in a multifarious environment. Mapping of intraclass land-cover types, such as the different stages of paddy, bare soil and wet soil, and different vegetation cover, will ordinarily be difficult without availability of intricating information in the image to discriminate one feature from another. This does not mean that SVM and RF are not satisfactory, they also perform well; however, they have no capability for attributing data decision intelligence. In

summary, the DM approach is a resourceful method for high-quality LULC mapping and will also be useful for mapping under different and more heterogeneous environment.

Acknowledgments

SPOT-6 and RADARSAT-2 data used for this study were provided by the Malaysian Remote Sensing Agency (ARSM). Our appreciations also to the Department of Town and Country Planning, Kuala Lumpur, for providing the land-use map of the study area.

References

1. M. B. A. Gibril et al., "Fusion of RADARSAT-2 and multispectral optical remote sensing data for LULC extraction in a tropical agricultural area," *Geocarto Int.* **32**, 735–748 (2017).
2. F. B. Sanli et al., "Evaluation of image fusion methods using PALSAR, RADARSAT-1 and SPOT images for land use/land cover classification," *J. Indian Soc. Remote Sens.* **45**, 591–601 (2017).
3. C. Hütt et al., "Best accuracy land use/land cover (LULC) classification to derive crop types using multitemporal, multisensor, and multi-polarization SAR satellite images," *Remote Sens.* **8**, 684 (2016).
4. M. I. Sameen et al., "A refined classification approach by integrating Landsat operational land imager (OLI) and RADARSAT-2 imagery for land-use and land-cover mapping in a tropical area," *Int. J. Remote Sens.* **37**, 2358–2375 (2016).
5. S. Chauhan and H. S. Srivastava, "Comparative evaluation of the sensitivity of multi-polarised SAR and optical data for various land cover," *Int. J. Adv. Remote Sens., GIS, Geogr.* **4**, 1–14 (2016).
6. V. Kumar, P. Agrawal, and S. Agrawal, "ALOS PALSAR and hyperion data fusion for land use land cover feature extraction," *J. Indian Soc. Remote Sens.* **45**(3), 407–416 (2017).
7. R. C. Estoque, Y. Murayama, and C. M. Akiyama, "Pixel-based and object-based classifications using high- and medium-spatial-resolution imageries in the urban and suburban landscapes," *Geocarto Int.* **30**, 1113–1129 (2015).
8. E. Hussain and J. Shan, "Object-based urban land cover classification using rule inheritance over very high-resolution multisensor and multitemporal data," *GISci. Remote Sens.* **53**, 164–182 (2016).
9. R. Momeni, P. Aplin, and D. S. Boyd, "Mapping complex urban land cover from spaceborne imagery: the influence of spatial resolution, spectral band set and classification approach," *Remote Sens.* **8**, 88 (2016).
10. A. Mui, Y. He, and Q. Weng, "An object-based approach to delineate wetlands across landscapes of varied disturbance with high spatial resolution satellite imagery," *ISPRS J. Photogramm. Remote Sens.* **109**, 30–46 (2015).
11. V. Moosavi et al., "Application of Taguchi method to satellite image fusion for object-oriented mapping of Barchan dunes," *Geosci. J.* **18**, 45–59 (2014).
12. H. Tong et al., "A supervised and fuzzy-based approach to determine optimal multi-resolution image segmentation parameters," *Photogramm. Eng. Remote Sens.* **78**, 1029–1044 (2012).
13. B. M. G. Ribeiro and L. M. G. Fonseca, "Urban land cover classification using WorldView-2 images and C4.5 algorithm," in *Joint Urban Remote Sensing Event (JURSE '11)*, pp. 250–253 (2013).
14. B. Pradhan, M. S. Tehrany, and M. N. Jebur, "A new semiautomated detection mapping of flood extent from TerraSAR-X satellite image using rule-based classification and taguchi optimization techniques," *IEEE Trans. Geosci. Remote Sens.* **54**, 4331–4342 (2016).
15. M. Idrees, H. Z. M. Shafri, and V. Saeidi, "Imaging spectroscopy and light detection and ranging data fusion for urban feature extraction," *Am. J. Appl. Sci.* **10**, 1575–1585 (2013).
16. X. Zhang et al., "Segmentation quality evaluation using region-based precision and recall measures for remote sensing images," *ISPRS J. Photogramm. Remote Sens.* **102**, 73–84 (2015).

17. B. Pradhan et al., "Data fusion technique using wavelet transform and Taguchi methods for automatic landslide detection from airborne laser scanning data and Quickbird satellite imagery," *IEEE Trans. Geosci. Remote Sens.* **54**(3), 1610–1622 (2016).
18. B. W. Heumann, "An object-based classification of mangroves using a hybrid decision tree-support vector machine approach," *Remote Sens.* **3**, 2440–2460 (2011).
19. C. Zhang and Z. Xie, "Data fusion and classifier ensemble techniques for vegetation mapping in the coastal everglades," *Geocarto Int.* **29**, 228–243 (2014).
20. M. B. A. Gibril, H. Z. M. Shafri, and A. Hamedianfar, "New semi-automated mapping of asbestos cement roofs using rule-based object-based image analysis and Taguchi optimization technique from WorldView-2 images," *Int. J. Remote Sens.* **38**, 467–491 (2017).
21. U. Peeroo, M. O. Idrees, and V. Saeidi, "Building extraction for 3D city modelling using airborne laser scanning data and high-resolution aerial photo," *S. Afr. J. Geomatics* **6**, 363–376 (2017).
22. Y. Liu et al., "Discrepancy measures for selecting optimal combination of parameter values in object-based image analysis," *ISPRS J. Photogramm. Remote Sens.* **68**, 144–156 (2012).
23. D. Liu and F. Xia, "Assessing object-based classification: advantages and limitations," *Remote Sens. Lett.* **1**, 187–194 (2010).
24. H. Zhang, J. E. Fritts, and S. A. Goldman, "Image segmentation evaluation: a survey of unsupervised methods," *Comput. Vision Image Understanding* **110**, 260–280 (2008).
25. B. Johnson and Z. Xie, "Unsupervised image segmentation evaluation and refinement using a multi-scale approach," *ISPRS J. Photogramm. Remote Sens.* **66**, 473–483 (2011).
26. I. Dronova et al., "Landscape analysis of wetland plant functional types: the effects of image segmentation scale, vegetation classes and classification methods," *Remote Sens. Environ.* **127**, 357–369 (2012).
27. Y. Gao et al., "Optimal region growing segmentation and its effect on classification accuracy," *Int. J. Remote Sens.* **32**, 3747–3763 (2011).
28. A. Smith, "Image segmentation scale parameter optimization and land cover classification using the random forest algorithm," *J. Spat. Sci.* **55**, 69–79 (2010).
29. C. Witharana and D. L. Civco, "Optimizing multi-resolution segmentation scale using empirical methods: exploring the sensitivity of the supervised discrepancy measure Euclidean distance 2 (ED2)," *ISPRS J. Photogramm. Remote Sens.* **87**, 108–121 (2014).
30. Z. Guo and S. Du, "Mining parameter information for building extraction and change detection with very high-resolution imagery and GIS data," *GISci. Remote Sens.* **54**, 38–63 (2017).
31. A. Räsänen et al., "What makes segmentation good? A case study in boreal forest habitat mapping," *Int. J. Remote Sens.* **34**, 8603–8627 (2013).
32. N. Clinton et al., "Accuracy assessment measures for object-based image segmentation goodness," *Photogramm. Eng. Remote Sens.* **76**, 289–299 (2010).
33. L. Draguţ, D. Tiede, and S. R. Levick, "ESP: a tool to estimate scale parameter for multiresolution image segmentation of remotely sensed data," *Int. J. Geogr. Inf. Sci.* **24**, 859–871 (2010).
34. P. R. Marpu et al., "Enhanced evaluation of image segmentation results," *J. Spat. Sci.* **55**, 55–68 (2010).
35. G. M. Espindola et al., "Parameter selection for region-growing image segmentation algorithms using spatial autocorrelation," *Int. J. Remote Sens.* **27**, 3035–3040 (2006).
36. M. Kim and M. Madden, "Determination of optimal scale parameters for alliance-level forest classification of multispectral IKONOS images," in *Proc. of the 1st Int. Conf. on Object-based Image Analysis (OBIA '06)* (2006).
37. T. R. Martha et al., "Segment optimization and data-driven thresholding for knowledge-based landslide detection by object-based image analysis," *IEEE Trans. Geosci. Remote Sens.* **49**, 4928–4943 (2011).
38. H. Luo et al., "Development of a multi-scale object-based shadow detection method for high spatial resolution image," *Remote Sens. Lett.* **6**, 59–68 (2015).
39. T. Kavzoglu, M. Y. Erdemir, and H. Tonbul, "A region-based multi-scale approach for object-based image analysis," in *Int. Archives of the Photogrammetry, Remote Sensing and Spatial Information Sciences*, Vol. 41, pp. 241–247 (2016).

40. V. Moosavi, A. Talebi, and B. Shirmohammadi, "Producing a landslide inventory map using pixel-based and object-oriented approaches optimized by Taguchi method," *Geomorphology* **204**, 646–656 (2014).
41. M. O. Idrees and B. Pradhan, "Hybrid Taguchi-objective function optimization approach for automatic cave bird detection from terrestrial laser scanning intensity image," *Int. J. Speleol.* **45**, 289–301 (2016).
42. R. S. Rao et al., "The Taguchi methodology as a statistical tool for biotechnological applications: a critical appraisal," *Biotechnol. J.* **3**, 510–523 (2008).
43. M. H. Shojaeefard et al., "Application of Taguchi optimization technique in determining aluminum to brass friction stir welding parameters," *Mater. Des.* **52**, 587–592 (2013).
44. Trimble, *Trimble eCognition Developer User Guide*, pp. 1–266, Trimble Navigation Limited, Westminster, USA (2014).
45. W. Yu et al., "A new approach for land cover classification and change analysis: integrating backdating and an object-based method," *Remote Sens. Environ.* **177**, 37–47 (2016).
46. M. O. Idrees and B. Pradhan, "Hybrid Taguchi-objective function optimization approach for automatic cave bird detection from terrestrial laser scanning intensity image," *Int. J. Speleol.* **45**, 289–301 (2016).
47. G. M. Espindola et al., "Parameter selection for region-growing image segmentation algorithms using spatial autocorrelation," *Int. J. Remote Sens.* **27**, 3035–3040 (2006).
48. M. O. Idrees et al., "Assessing the transferability of a hybrid Taguchi-objective function method to optimize image segmentation for detecting and counting cave roosting birds using terrestrial laser scanning data," *J. Appl. Remote Sens.* **10**, 035023 (2016).
49. B. Pradhan et al., "Data Fusion technique using wavelet transform and Taguchi methods for automatic landslide detection from airborne laser scanning data and Quickbird satellite imagery," *IEEE Trans. Geosci. Remote Sensing* **54**, 1–13 (2015).
50. A. Reyes, M. Solla, and H. Lorenzo, "Comparison of different object-based classifications in LandsatTM images for the analysis of heterogeneous landscapes," *Meas. J. Int. Meas. Confed.* **97**, 29–37 (2017).
51. M. Belgiu and L. Drăgu, "Random forest in remote sensing: a review of applications and future directions," *ISPRS J. Photogramm. Remote Sens.* **114**, 24–31 (2016).
52. F. J. Aguilar et al., "A quantitative assessment of forest cover change in the Moulouya River watershed (Morocco) by the integration of a subpixel-based and object-based analysis of Landsat data," *Forests* **7**, 23 (2016).
53. M. P. dos Santos Silva et al., "Remote-sensing image mining: detecting agents of land-use change in tropical forest areas," *Int. J. Remote Sens.* **29**, 4803–4822 (2008).
54. P. Thamilselvana and J. G. R. Sathiaseelan, "A comparative study of data mining algorithms for image classification," *Int. J. Educ. Manage. Eng.* **5**, 1–9 (2015).
55. M. A. Vieira et al., "Object based image analysis and data mining applied to a remotely sensed Landsat time-series to map sugarcane over large areas," *Remote Sens. Environ.* **123**, 553–562 (2012).
56. B. Salehi et al., "Object-based classification of urban areas using VHR imagery and height points ancillary data," *Remote Sens.* **4**, 2256–2276 (2012).
57. J. Nichol and M. S. Wong, "Habitat mapping in rugged terrain using multispectral ikonos images," *Photogramm. Eng. Remote Sens.* **74**, 1325–1334 (2008).
58. G. M. Foody, "Thematic map comparison: evaluating the statistical significance of differences in classification accuracy," *Photogramm. Eng. Remote Sens.* **70**, 627–633 (2004).
59. M. B. A. Gibril et al., "Fusion of RADARSAT-2 and multispectral optical remote sensing data for LULC extraction in a tropical agricultural area," *Geocarto Int.* **32**(7), 735–748 (2016).
60. T. R. Martha et al., "Segment optimization and data-driven thresholding for knowledge-based landslide detection by object-based image analysis," *IEEE Trans. Geosci. Remote Sens.* **49**, 4928–4943 (2011).

Mohamed Barakat A. Gibril graduated with a first-class honors degree in surveying (geodesy) from Sudan University of Science and Technology, Khartoum, Sudan, in 2010. He completed his

master's degree in remote sensing and GIS from Universiti Putra Malaysia in 2015. He is currently a lecturer at the University of Prince Mugrin, Madinah, Saudi Arabia. His research focuses on satellite image analysis, data fusion, urban mapping from very high-resolution satellite imageries, data mining, and geographic object-based image analysis.

Mohammed Oludare Idrees graduated with distinction in surveying and geoinformatics from Federal Polytechnic, Ado-Ekiti, Nigeria. He obtained his master's degree in remote sensing and GIS and PhD degree in GIS and geomatic engineering from Universiti Putra Malaysia in 2013 and 2017, respectively. He has over 5 years of industrial and more than 3 years of teaching experience. He has published over 25 research papers in refereed technical journals. His research interests are satellite image analysis and spatial modeling.

Kouame Yao obtained his bachelor's degree in computing in 2009 from UCSI University, Malaysia and a master's degree in information technology management in 2011 from Staffordshire, United Kingdom. Inspired by the growing application of information technology in geosciences, he obtained two master's degrees in remote sensing and GIS from Universiti Putra Malaysia and geosciences from Macquarie University, Australia, in 2015 and 2018, respectively. His research interest is in application of remote sensing in mineral exploration.

Helmi Zulhaidi Mohd Shafri graduated with a first-class honors degree in surveying from RMIT University, Melbourne, Australia, in 1998. He completed his PhD degree in remote sensing from the University of Nottingham, United Kingdom, in 2003. Now, he is the coordinator of the remote sensing and GIS program at the Faculty of Engineering, UPM. He is actively involved in research related to algorithm development and new applications of remote sensing especially in urban engineering and environmental-informatics areas. He has more than 12 years of teaching, research, administrative, and consultancy experience with more than 80 papers in refereed technical journals.